Redox Mechanisms Involved in the Selective Activation of Nrf2-mediated Resistance *Versus* p53-dependent Apoptosis in Adenocarcinoma Cells*

Sara Piccirillo[‡1], Giuseppe Filomeni[§1], Bernhard Brüne[¶], Giuseppe Rotilio[‡§], and Maria R. Ciriolo[‡§2]

From the §Department of Biology, University of Rome "Tor Vergata," Via della Ricerca Scientifica, 1, 00133 Rome, Italy, the ¶Institute of Biochemistry I/ZAFES, Faculty of Medicine, Johann Wolfgang Goethe University, Theodor-Stern-Kai, 7, 60590 Frankfurt, Germany, and the ‡Research Centre IRCCS San Raffaele-Pisana, Via dei Bonacolsi, 00163 Rome, Italy

We have investigated the role of reactive oxygen species and thiol-oxidizing agents in the induction of cell death and have shown that adenocarcinoma gastric (AGS) cells respond differently to the oxidative challenge according to the signaling pathways activated. In particular, apoptosis in AGS cells is induced via the mitochondrial pathway upon treatment with thiol-oxidizing agents, such as diamide. Apoptosis is associated with persistent oxidative damage, as evidenced by the increase in carbonylated proteins and the expression/activation of DNA damage-sensitive proteins histone H2A.X and DNA-dependent protein kinase. Resistance to hydrogen peroxide is instead associated with Keap1 oxidation and rapid translocation of Nrf2 into the nucleus. Sensitivity to diamide and resistance to hydrogen peroxide are correlated with GSH redox changes, with diamide severely increasing GSSG, and hydrogen peroxide transiently inducing protein-GSH mixed disulfides. We show that p53 is activated in response to diamide treatment by the oxidative induction of the Trx1/p38^{MAPK} signaling pathway. Similar results were obtained with another carcinoma cell line, CaCo2, indicating that these findings are not limited to AGS cells. Our data suggest that thiol-oxidizing agents could be exploited as inducers of apoptosis in tumor histotypes resistant to ROS-producing chemotherapeutics.

Reactive oxygen species (ROS),[3] constantly generated by all aerobic organisms, are involved in many physiological functions and in pathological processes, such as cancer. Recent studies have shown that cancer cells produce higher levels of ROS than normal cells because of both intense metabolic activity and mitochondrial defects (1). This intrinsic oxidative stress selectively targets malignant cells for therapeutic strategies based on further ROS production and the consequent irreversible oxidative insult (2). Indeed, several anticancer drugs commonly used in chemotherapy (*e.g.* adriamycin and cisplatin) are able to induce a site-directed burst of ROS as a part of their mechanism of action, which is particularly detrimental for tumor cells (3). However, for the efficiency of ROS-based treatments, expression of antioxidants and activation of redox-sensitive transduction pathways must also be considered.

It is now well established that ROS participate in the control of phosphorylative cascades and transcription activity (4). In fact, the cell response to pro-oxidant stimuli is often accompanied by direct modification of highly conserved cysteine residues on proteins, normally present in the reduced form, that act as "redox sensors." Among the proteins that possess this regulatory function, thioredoxin 1 (Trx1) is a well characterized example (5). The identification of Trx1 as an interactor of apoptosis signal-regulating kinase 1 (ASK1), which is responsible for the activation of p38^{MAPK} and c-Jun N-terminal kinase (JNK) upstream kinases (6), sheds new light on the possible cross-talk between phosphorylative and redox regulation modes (7). Moreover, a growing amount of data demonstrates that the reduced state of specific cysteines of several transcription factors is maintained by proteins such as Trx1 to ensure the DNA binding capability (8). The nuclear erythroid factor 2-related factor 2 (Nrf2) is a typical activator of antioxidant-responsive elements (AREs) (9) that, once activated, induces the antioxidant and detoxifying response (10, 11). Nrf2 is normally sequestered in the cytoplasm in an inactive complex with kelch-like ECH-associated protein 1 (Keap1), which, upon oxidation of critical cysteines, dissociates from Nrf2, leading to its translocation into the nucleus (12).

The tumor suppressor p53 is another redox-sensitive transcription factor involved in DNA repair from genotoxic damages and in induction of apoptosis (13). For a correct binding to DNA, p53 has to be previously stabilized and activated, then it can translocate into the nucleus and undergo modulation of its redox state (14). This modulation seems to be related to the oxidation of Trx1, which leads to the nuclear accumulation of p53 in the active form and determines the trans-activation of downstream genes (15). Recently, a negative effect on Nrf2 transcriptional activity mediated by p53 has been characterized. Under basal conditions, direct binding of p53 to ARE-containing promoters is able to counteract Nrf2 activity. Under mild oxidative stress, the cross-talk between these two transcription factors regulates the induc-

tion of a strong antioxidant response, thus modulating the downstream induction of apoptosis (16).

Adenocarcinoma gastric (AGS) cells represent a good model to study resistance to ROS. The high basal levels of S-glutathionylated proteins and their role in mediating the response to oxidative stress represent the principal mechanism of this resistance (17). In the present article, we dissect the molecular mechanisms of different oxidizing molecules in inducing survival or the apoptotic response by activating Nrf2 or p53 in adenocarcinoma cells, giving a rationale for the specific activation of their downstream signaling pathways.

EXPERIMENTAL PROCEDURES

Materials—Diamide, dithionitrobenzoate (DTNB), dimethyl sulfoxide, H_2O_2, paraquat, propidium iodide, goat anti-mouse, and anti-rabbit IgG (H+L)-horseradish peroxidase conjugate were from Sigma. GSH and GSSG were from Roche Applied Science. The OxyBlot detection kit was from Intergen (Purchase, NY). Nitrocellulose membrane was from Bio-Rad. Alexa Fluor 568-conjugated secondary antibody and Alexa Fluor 488-conjugated secondary antibody were from Molecular Probes (Eugene, OR). ChemiGlow chemiluminescence substrate was from Alpha Innotech Corporation (San Leandro, CA). All other chemicals were from Merck.

Cell Cultures—Human AGS and CaCo2 cells were purchased from the European Collection of Cell Culture and grown at 37 °C in an atmosphere of 5% CO_2 in F12 medium and Dulbecco's modified Eagle's medium, respectively, supplemented with 10% fetal calf serum, 2 mM L-glutamine, and 0.1% penicillin/streptomycin (Lonza, Milan, Italy).

Treatments—The solutions of diamide (20 mM) and DTNB (20 mM) were prepared in dimethyl sulfoxide. The solutions of paraquat (200 mM), xanthine (100 mM), and H_2O_2 (200 mM) were prepared in water. All solutions were prepared just before the experiments, and treatments were done for 1 h with different concentrations ranging from 50 μM to 2 mM in serum-containing medium. Then, the medium was removed, cells were washed, and recovery was followed. Treatment with xanthine/xanthine oxidase was performed adding 0.1 unit/ml enzyme. Different concentrations of the substrate were added every 15 min for 1 h. As a control, equal volumes of dimethyl sulfoxide (0.1%) or water were added to untreated cells. Buthionine sulfoximine (BSO) was used at a concentration of 1 mM, added 12 h before treatments, and maintained throughout the experiments. *N*-Acetylcysteine (CysNAc) was added to the culture medium at a concentration of 5 mM, 1 h before treatments, and maintained throughout the experiments. Cell-permeable JNK and p38^{MAPK} inhibitors SP600125 and SB203580 (Calbiochem-Novabiochem) were added at concentrations of 10 and 15 μM, respectively, for 1 h before the addition of diamide, maintained during treatment, and readded during recovery.

Analysis of Cell Viability and Apoptosis—After 24 h of recovery, adherent and detached cells were combined and stained with 50 μg/ml propidium iodide prior to analysis by a FACScalibur instrument (BD Biosciences). Apoptotic cells were evaluated by calculating peak areas of hypodiploid nuclei (sub-G_1) (18). Alternatively, cells were counted after trypan blue staining by optic microscopy.

Western Blot Analyses—Total and nuclear extracts were obtained as reported previously (19), electrophoresed by SDS-PAGE, and blotted onto nitrocellulose or polyvinylidene difluoride membrane (Bio-Rad). Polyclonal anti-caspase-9, anti-phospho-p38^{MAPK} (Thr^{180}/Tyr^{182}), and monoclonal anti-caspase-3 were obtained from Cell Signaling Technology (Beverly, MA). Polyclonal anti-actin, anti-Nrf2, anti-SOD1, anti-Bax, anti-p38^{MAPK}, anti-JNK1, monoclonal anti-poly-(ADP-ribose) polymerase (PARP), anti-histone H2B, anti-Keap1, and anti-phospho-JNK were from Santa Cruz Biotechnology (Santa Cruz, CA). Monoclonal anti-p53 and anti-catalase were from Sigma. Polyclonal anti-DNA-PK (StressGen, VWR International, Milan, Italy). Monoclonal anti-phospho-H2A.X was from Upstate Biotechnology (Lake Placid, NY). Monoclonal anti-lamin A/C was from UCS Diagnostic (Rome, Italy). Monoclonal anti-heme oxygenase-1 (BD Biosciences) was used as primary antibody. The specific protein complex, formed upon incubation with specific secondary antibodies, was identified using a Fluorchem imaging system (Alpha Innotech) after incubation with ChemiGlow chemiluminescence substrate.

Redox Western Blotting—The Keap1 redox state was analyzed as described previously (20). Briefly, cells were treated with cold trichloroacetic acid at final concentration of 10% for 30 min at 4 °C. Proteins were then precipitated at $12,000 \times g$ for 10 min, and pellets were incubated for 30 min in cold acetone at 4 °C. Further, pellets were dissolved in 20 mM Tris/HCl (pH 8.0) containing 15 mM AMS (Molecular Probes) and incubated at room temperature for 3 h to allow modifying free thiols. Keap1 redox forms were then separated on 7.5% SDS-PAGE in nonreducing loading buffer and blotted onto nitrocellulose or polyvinylidene difluoride. Polyclonal anti-Keap1 was used as primary antibody. The Trx1 redox state was determined by urea-PAGE as described previously (21). Briefly, cells were lysed in urea buffer (8 M urea, 100 mM Tris (pH 8.2), 1 mM EDTA) containing 30 mM iodoacetic acid to carboxymethylate protein sulfhydryls. After 15 min at 37 °C, iodoacetic acid was removed by precipitation with acetone and 1 N HCl (98:2 v/v) followed by centrifugation. Reduction of protein disulfides was achieved in urea buffer with 3.5 mM dithiothreitol for 30 min at 37 °C. After reduction, newly generated thiols were amidomethylated by the addition of 10 mM iodoacetamide. Proteins were separated on a 9% urea-polyacrylamide gel and blotted onto polyvinylidene difluoride. Polyclonal anti-Trx1 (Santa Cruz Biotechnology) was used as primary antibody.

Cell Transfections—Twenty-four hours after plating, AGS cells were transfected with a small interference RNA (siRNA) against p53, as previously described (19), or with a SignalSilence® Pool p38^{MAPK} siRNA (sip38^{MAPK}) (Cell Signaling Technology). Control cells were transfected with a scramble siRNA duplex (siScr), which does not present homology with any other human mRNAs. AGS cells were transiently transfected with pmaxFP^{TM}-Green-C empty vector or pmaxFP^{TM}-Green-C containing the dominant negative Nrf2 protein (DN-Nrf2) by electroporation using a GenePulser Xcell system (Bio-Rad). Transfection efficiency was estimated by analyzing green fluorescence of the maxFP^{TM}-Green epitope. Experiments with a transfection efficiency >80% were considered. CaCo2 cells were transfected with a pcDNA3 empty vector

TABLE 1

Dose response of AGS cells to different pro-oxidants

AGS cells were plated at a density of $2 \times 10^4/cm^2$ and treated with the indicated concentrations of paraquat, xanthine/xanthine oxidase, hydrogen peroxide, DTNB, and diamide for 1 h. Cells were then transferred to fresh medium for 24 h, washed, and stained with propidium iodide. Analysis of cell cycle and apoptosis was performed by a FACScalibur instrument, and percentages of positive-staining cells were calculated using WinMDI version 2.8 software. Values reported represent the mean $\pm$ S.D. of $n = 5$ independent experiments.

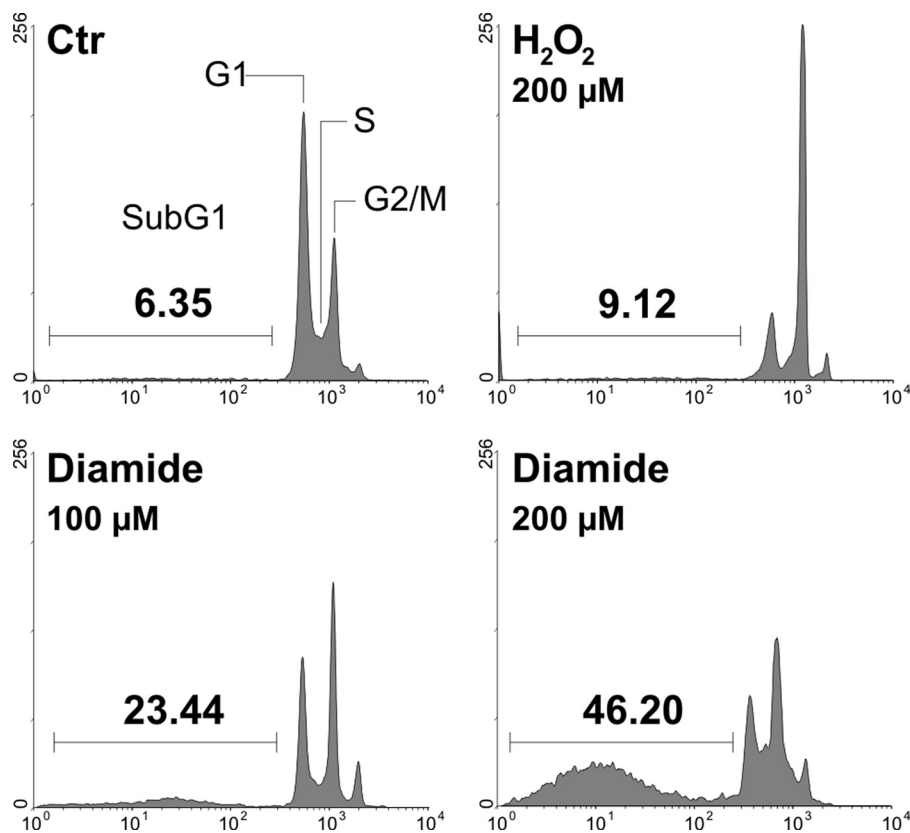| Paraquat		Xanthine/ xanthine oxidase		Hydrogen peroxide		DTNB		Diamide	
Conc.	Apoptosis	Conc.	Apoptosis	Conc.	Apoptosis	Conc.	Apoptosis	Conc.	Apoptosis
M	*%*	*mM*	*%*	*mM*	*%*	*mM*	*%*	*mM*	*%*
0	6.65 ± 2.11	0	5.84 ± 1.35	0	5.68 ± 1.00	0	5.91 ± 1.12	0	6.12 ± 2.08
0.5	8.59 ± 1.78	0.25	5.19 ± 2.33	0.1	8.59 ± 0.92	0.05	18.30 ± 3.62	0.05	21.19 ± 3.19
1.0	9.86 ± 2.99	0.5	4.76 ± 1.83	0.2	9.86 ± 2.65	0.1	22.44 ± 3.63	0.1	25.76 ± 4.06
2.0	11.70 ± 3.03	1.0	6.96 ± 1.45	0.5	11.91 ± 3.12	0.2	35.77 ± 5.91	0.2	46.96 ± 4.41

FIGURE 1. **AGS cells show different sensitivity toward pro-oxidant compounds.** AGS cells were plated at a density of $2 \times 10^4/cm^2$ and treated with 200 μM H$_2$O$_2$ or 100 μM or 200 μM diamide for 1 h. *Ctr*, control. Cells were then transferred to fresh medium for 24 h, washed, and stained with propidium iodide. Analyses of cell cycle and apoptosis were performed with a FACScalibur instrument, and percentages of positive-staining cells were calculated using WinMDI version 2.8 software. Cell cycle plots reported are from a typical experiment done in triplicate of five that gave similar results.

Fluorescence Microscopy Analyses— Cells were cultured on coverslips, fixed with 4% paraformaldehyde, and permeabilized. Monoclonal anti-cytochrome *c*, polyclonal anti-Hsp60, and polyclonal anti-Nrf2 (Santa Cruz Biotechnology), monoclonal anti-Ser[139]-phosphorylated histone H2A.X (Upstate Biotechnology), monoclonal anti-p53 (Sigma), polyclonal anti-phospho-p38[MAPK] (Thr[180]/Tyr[182]) (Cell Signaling) were used as primary antibodies and probed successively with the appropriate Alexa Fluor 568- or Alexa Fluor 488-conjugated secondary antibody. To visualize nuclei and the actin cytoskeleton, cells were incubated with the cell-permeable DNA-specific dye Hoechst 33342 (Calbiochem-Novabiochem) and fluorescein isothiocyanate-conjugated phalloidin (Invitrogen), respectively. Images were digitized either with a Cool Snap video camera connected to a Nikon Eclipse TE200 fluorescence microscope or with a Delta Vision Restoration microscopy system (Applied Precision, Inc., Issaquah, WA) equipped with an Olympus IX70 fluorescence microscope. Proteins were determined by the method of Lowry *et al.* (23).

(mock) or with a pcDNA3 vector containing the coding sequence for WTp53. Cells were used at 48 h from transfection because this time was sufficient to increase the expression of p53 significantly, as evidenced by Western blot analysis.

*Measurement of Glutathione and Protein Carbonyls—*Intracellular GSH, GSSG, and glutathione mixed disulfides (GS-R) were assayed by HPLC as described previously (22). Data are expressed as nanomoles of GSH equivalents/mg of protein. Carbonylated proteins were detected using the OxyBlot detection kit. Briefly, 20 μg of proteins were reacted with 2,4-dinitrophenylhydrazine (DNP) for 15 min at 25 °C. Samples were resolved on 12% SDS-PAGE, and DNP-derivatized proteins were identified by immunoblotting using an anti-DNP antibody.

*Data Presentation—*All experiments were done at least three different times unless otherwise indicated. The results are presented as means $\pm$ S.D. Statistical evaluation was conducted by analysis of variance followed by Bonferroni's test. Differences were considered to be significant at $p < 0.05$.

RESULTS

*AGS Cells Show Different Sensitivity toward Different Pro-oxidant Compounds—*The responses of AGS cells to oxidative stress were studied by treating the cells with two different classes of pro-oxidant molecules: the first was formed by H$_2$O$_2$ and ROS producers (paraquat and xanthine/xanthine oxidase);
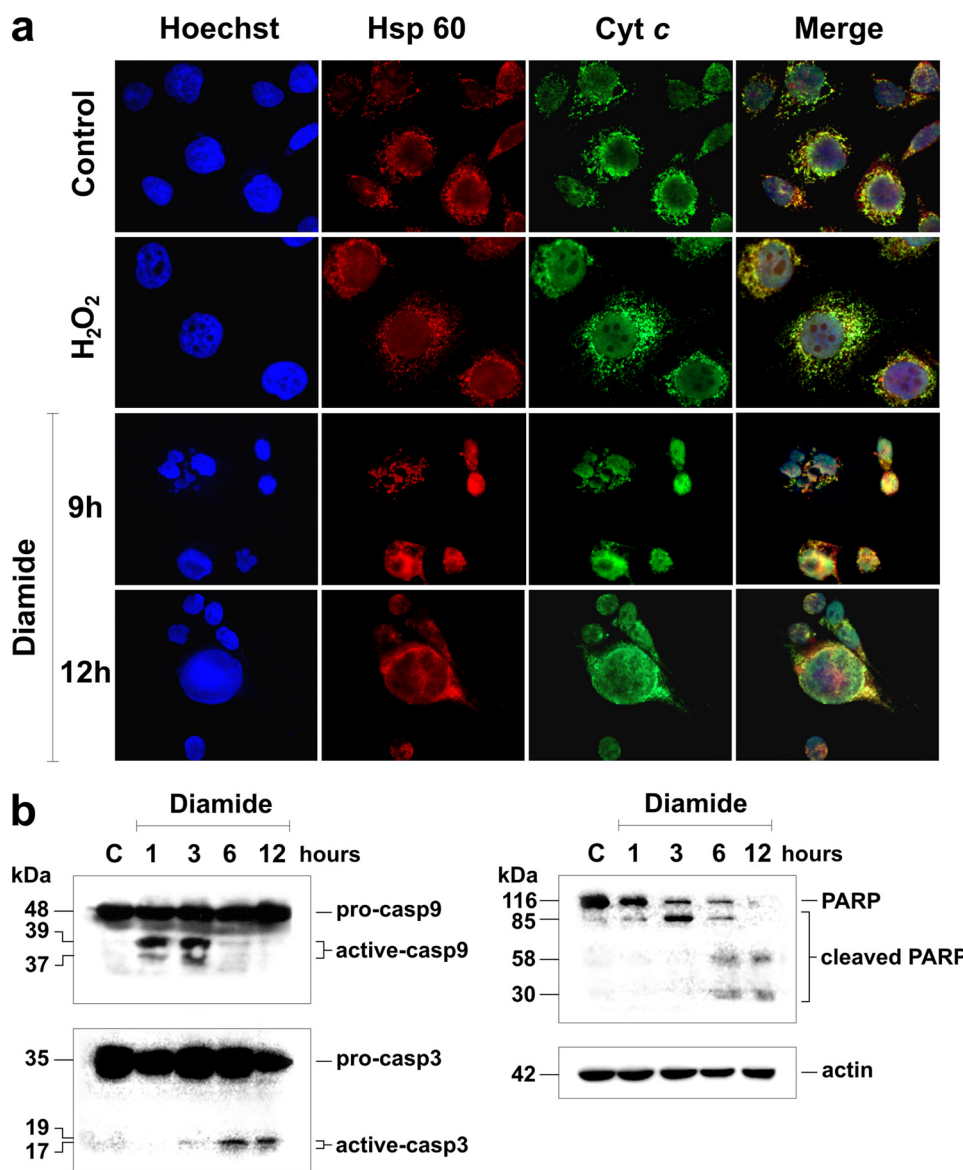
a

b

FIGURE 2. **AGS cells undergo diamide-mediated apoptosis via the mitochondrial pathway.** AGS cells were treated with 200 μM H_2O_2 or diamide for 1 h and transferred to fresh medium. *a*, after recovery from H_2O_2 (12 h) or diamide (9 and 12 h), cells were fixed with *p*-formaldehyde and subjected to immunostaining with an anti-Hsp60 antibody (*red*) and an anti-cytochrome *c* (*Cyt c*) antibody (*green*). Nuclei (*blue*) were stained with Hoechst 33342. Images reported are from one experiment of three that gave similar results. *b*, at the indicated times of recovery, cells were lysed, and 30 μg of total cell extracts were loaded for the immunodetection of caspase-3 (*casp3*), caspase-9 (*casp9*), and PARP. Actin was used as loading control. Immunoblots are from one experiment representative of three that gave similar results.

Data show that H_2O_2 at 200 μM did not increase the percentage of sub-G_1 (apoptotic) cell population, but only resulted in a sustained cell cycle arrest in G_2/M phase. Conversely, treatment with diamide efficiently activated apoptosis, the extent of which was dose-dependent and reached values close to 50% for a concentration of 200 μM. Similar results were also obtained by direct cell counts after trypan blue staining (data not shown). On the basis of these results, we selected the concentration of 200 μM for both compounds.

AGS Cells Undergo Diamide-mediated Apoptosis via the Mitochondrial Pathway—To characterize the mechanisms underlying apoptosis after diamide treatment, we analyzed the involvement of the mitochondrial pathway. Cells were incubated with 200 μM diamide or H_2O_2 for 1 h and then analyzed for the activation of apoptotic markers at different times of recovery. Fig. 2*a* shows fluorescence microscopy analyses of cells stained with an antibody anti-Hsp60, a mitochondria-specific chaperone, to localize mitochondria, and with an antibody anti-cytochrome *c*. Although no difference was observed between control and H_2O_2-treated cells, Hsp60 did not superimpose cytochrome *c* staining upon treatment with diamide, indicating that cytochrome *c* was efficiently released from mitochondria into the cytosol. Concomitantly, Western blot analyses of caspase-9, caspase-3, and PARP indicated that each step of the apoptotic program was executed upon treatment with diamide (Fig. 2*b*). In particular, proteolysis and activation of caspases and PARP were detected as sequential events, starting from the upstream caspase-9 (1–3 h) and going through caspase-3 and PARP (6–12 h).

Diamide and H_2O_2 Affect the Intracellular Sulfydryl Pool Differently—We focused on the possible modulation of GSH that, being the major non-protein thiol in cells, preferentially reacts with diamide. Moreover, GSH is the cofactor required for glutathione peroxidase to reduce H_2O_2, and it is a direct ROS scavenger. AGS cells were incubated with 200 μM H_2O_2 or diamide, and the change of GSH status was determined by analyzing the intracellular levels of GSH, GSSG, and mixed disulfides between GSH and proteins (GS-R). Fig. 3*a* shows that, under basal conditions, AGS cells had high levels of GS-R, as we reported previously (17). Upon

the second included thiol-oxidizing compounds (DTNB and diamide). To avoid prolonged oxidative stress, which could result in widespread damage, cells were treated for 1 h with each compound and transferred to fresh medium for recovery or for analysis of the signal transduction pathways involved in the response to redox unbalance. First, we analyzed the occurrence of apoptosis after 24 h of recovery. Results obtained from these experiments indicated that AGS cells were particularly resistant to ROS; in contrast, extensive cell death was seen upon treatment with agents that oxidize cellular thiols (Table 1). Therefore, we selected H_2O_2 and diamide as representative of the two classes of stressors and as examples of cell resistance *versus* sensitivity to oxidative burst. Fig. 1 shows cytofluorometric histograms of AGS cells treated with H_2O_2 or diamide.
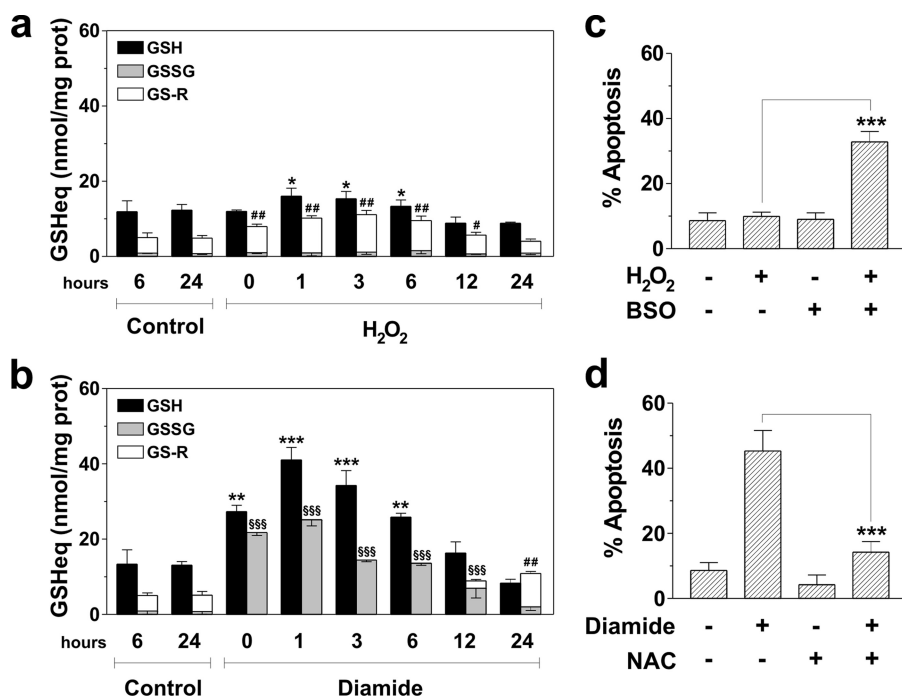
FIGURE 3. **Diamide and H_2O_2 affect the intracellular sulfhydryl pool differently.** *a* and *b*, AGS cells were treated with 200 μM H_2O_2 (*a*) or diamide (*b*) for 1 h and transferred to fresh medium. At the indicated times of recovery, cells were collected, washed exhaustively with phosphate-buffered saline, and used for GSH, GSSG, and GS-R assay by HPLC. GSH, GSSG, and GS-R data are expressed as nanomoles of GSH_{eq}/mg of total protein. Values represent means ± S.D. (*n* = 5). For GSH: *, $p < 0.05$; **, $p < 0.01$; ***, $p < 0.001$. For GS-R: #, $p < 0.05$; ##, $p < 0.01$. For GSSG: §§§, $p < 0.001$. *c*, AGS cells were incubated with 1 mM BSO for 12 h and then treated with 200 μM H_2O_2. After 1 h of treatment, cells were transferred to fresh medium containing 1 mM BSO, cultured for an additional 24 h, and finally stained with propidium iodide for cytofluorometric analysis of apoptosis. Data are expressed as means ± S.D. (*n* = 5). ***, $p < 0.001$. *d*, AGS cells were incubated with 5 mM CysNAc (*NAC*) for 1 h and then treated with 200 μM diamide. After 1 h of treatment, cells were transferred to fresh medium containing 5 mM CysNAc, cultured for an additional 24 h, and finally stained with propidium iodide for cytofluorometric analysis of apoptosis. Data are expressed as means ± S.D. (*n* = 5). ***, $p < 0.001$.

treatment with H_2O_2, GS-R and GSH contents transiently increased, to reach maximum values at 3–6 h of recovery, whereas no significant changes in GSSG were observed throughout the experiment. In particular, the GS-R increase preceded that of GSH, suggesting a dynamic equilibrium between these species in response to protein oxidation. Conversely, treatment with diamide induced a drastic increase of both GSH (from 13 to 40 nmol/mg of protein) and GSSG (from 0.75 to 26 nmol/mg of protein) in the first hour of recovery. Moreover, GS-R decreased under the limit of detection during the first 6 h of recovery to rise later on, when cells underwent apoptosis (Fig. 3*b*), confirming the prominent capacity of diamide to oxidize GSH.

We lowered the concentration of GSH by incubating the cells for 12 h with BSO, a specific inhibitor of GSH synthesis, prior to treatment with 200 μM H_2O_2. Fig. 3*c* shows that BSO induced a significant increase in the number of sub-G_1 cells, confirming the efficiency of GSH in counteracting H_2O_2 toxicity.

To confirm that the effect of diamide was due to interference with cell thiols, we incubated the cells with 5 mM CysNAc, a well established thiol-reducing compound. Fig. 3*d* shows that Cys-NAc significantly rescued AGS cells from diamide-induced apoptosis, indicating that the availability of free sulfydryls is fundamental for cell survival.

Cell Responses Were Associated with Oxidative Damage to Macromolecules—The occurrence of the oxidative damage produced either by H_2O_2 or diamide was then determined. Fig.

4*a* shows that the incubation with 200 μM H_2O_2 gave rise to a minor increase in carbonylated proteins, which was buffered already after 3 h of recovery. Conversely, treatment with 200 μM diamide brought on a sustained increase of carbonylated proteins, with a maximum at 1 h, which only returned to control values after 12 h from diamide removal.

Damage to DNA was monitored by fluorescence microscopy analysis of phospho-activated histone H2A.X. Fig. 4*b* shows that, after 3 h of recovery, the appearance of H2A.X phosphorylated at Ser[139] (the activated isoform of the protein) could be evidenced upon treatment with H_2O_2. However, immunofluorescence of AGS cells incubated with diamide revealed a more pronounced increase of nuclear foci, which indicated a massive DNA double-strand break. This result was also confirmed by Western blot analyses of nuclear extracts obtained at 3 h of recovery, which showed a strong increment in the immunoreactive band of P-H2A.X after treatment with diamide (Fig. 4*c*) of >8-fold with respect to H_2O_2 (see densitometric analysis in Fig. 4*c, lower panel*).

The nuclear damage was further characterized by analyzing the activation of the DNA-PK. Although this activation relies on several events, an increase in the expression levels of the catalytic subunit of the enzyme (DNA-PKcs) is considered confirmatory of DNA-PK activation (24). Fig. 4*d* shows the Western blot analysis of DNA-PKcs on total cell lysates after treatment with H_2O_2 or diamide. Analyses of the 450 kDa immunoreactive band of DNA-PKcs, representative of the full-size protein, showed a time-dependent increase after treatment with H_2O_2, reaching values 50% higher than control; conversely, diamide induced a gradual decrease continuing for up to 12 h of recovery. Furthermore, for both treatments, a low molecular mass band (~170 kDa), which has been previously reported as an apoptosis-related cleaved form of DNA-PKcs (25), appeared, although with different kinetics and extent. This degradation product was faintly visible only at 30 min after H_2O_2 treatment and completely disappeared afterward, whereas after diamide treatment the yield was higher and remained sustained for up to 3 h.

H_2O_2 and Diamide Specifically Modulate Nrf2 or p53 in AGS Cells—We analyzed p53 and Nrf2, transcription factors that sense oxidative stress and mediate opposite responses downstream. In particular, we analyzed the expression and nuclear localization of p53 and Nrf2 after treatment with H_2O_2 or diamide. Fig. 5*a* shows Western blots of cytosolic and nuclear frac-
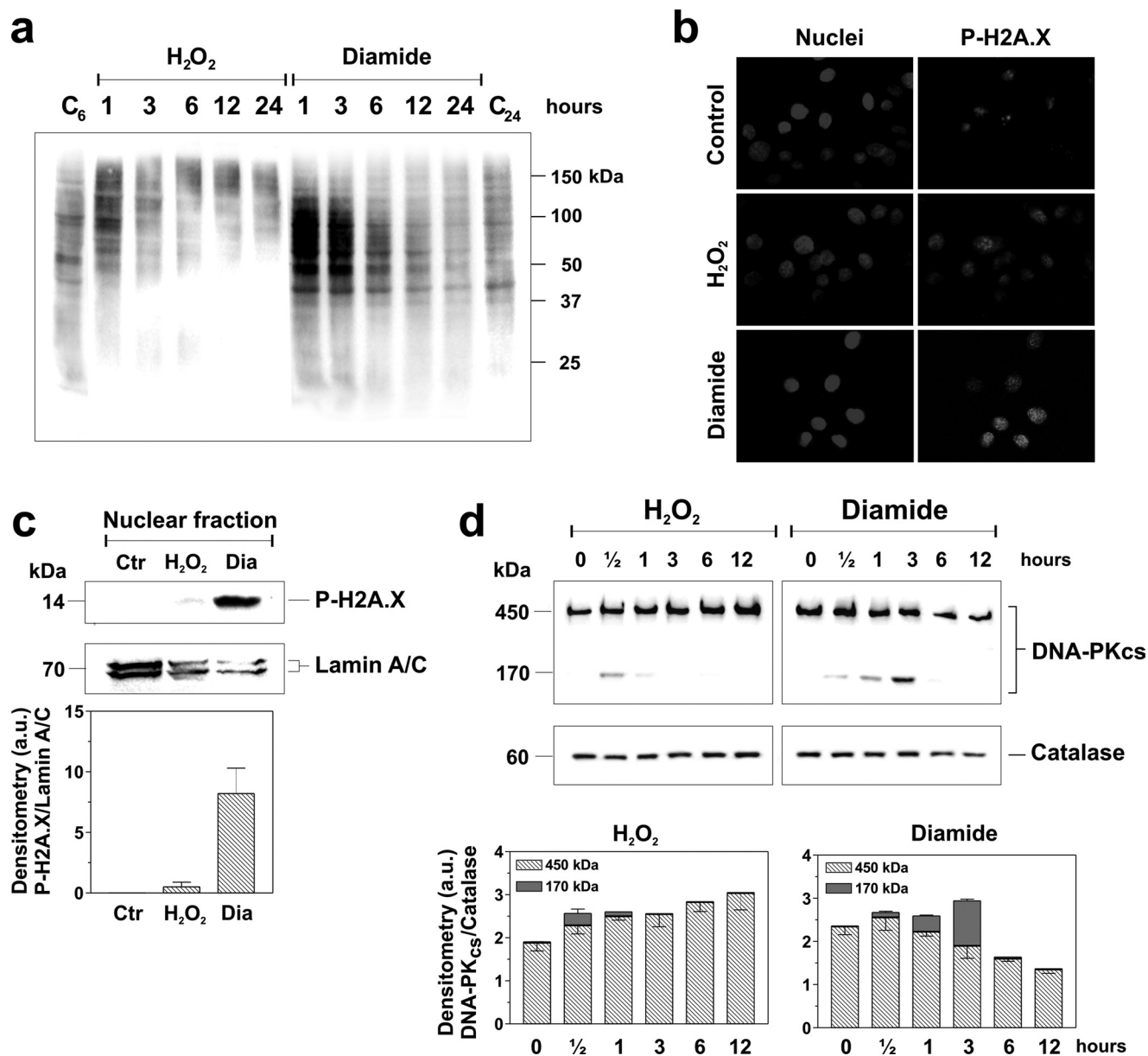
a

b

c

d

FIGURE 4. **Cell responses were associated with oxidative damage to macromolecules.** AGS cells were treated with 200 μM H_2O_2 or diamide for 1 h and transferred to fresh medium. *a*, at the indicated times of recovery, cells were lysed. Five micrograms of protein extracts were derivatized with DNP, and protein carbonyls were detected by Western blot analysis using an anti-DNP antibody. The immunoblot reported is representative of four that gave similar results. *b*, after 3 h of recovery cells, were fixed with *p*-formaldehyde and subjected to immunostaining with an anti-p-H2A.X antibody (*red*). Nuclei (*blue*) were stained with Hoechst 33342. Images reported are from one experiment of three that gave similar results. *c*, after 3 h of recovery, nuclear fraction was purified. Thirty micrograms of nuclear cell extracts were loaded for detection of p-H2A.X levels. Lamin A/C was used as loading control (*Ctr*). Immunoblots are from one experiment representative of three that gave similar results. Density of immunoreactive bands (reported below the immunoblots) was calculated using the software Quantity One (Bio-Rad), normalized for lamin A/C, and reported as arbitrary units (*a.u.*). Data are expressed as means $\pm$ S.D. ($n = 3$). *d*, at indicated the times of recovery, cell were lysed. Five micrograms of total cell extracts were loaded for detection of DNA-PKcs levels. Catalase was used as loading control. Immunoblots are from one experiment representative of three that gave similar results. Density of immunoreactive bands (reported below the immunoblot) was calculated using the software Quantity One, normalized for catalase, and reported as arbitrary units. Data are expressed as means $\pm$ S.D. ($n = 3$).

tions of both transcription factors. Nrf2 accumulated very early within the nuclear fraction only upon treatment with H_2O_2, whereas it did not translocate into the nucleus when AGS cells were treated with diamide. Interestingly, p53 showed completely opposite behavior by accumulating into the nucleus at early times upon diamide addition but not upon H_2O_2 treatment. It is worth noting that the high molecular mass band of Nrf2, which has been suggested to represent the 100-kDa Nrf2/actin active dimer (26), was observed mainly in the nuclear compartment. We also performed fluorescence microscopy

analyses of the localization of both transcription factors in AGS cells after 3 h from H_2O_2 or diamide treatment. Fig. 5*b* shows that H_2O_2 induced a stronger mobilization of Nrf2 from the actin filaments network, into the nucleus, whereas this occurred at lower extent upon diamide treatment. Interestingly, no superimposition between F-actin and Nrf2 could be observed after exposure to H_2O_2, and a peripheral localization of Nrf2 in discrete spots was evident under diamide treatment. The opposite behavior was visualized for p53; in fact, H_2O_2 caused only a slight increase in nuclear fluorescence of p53,
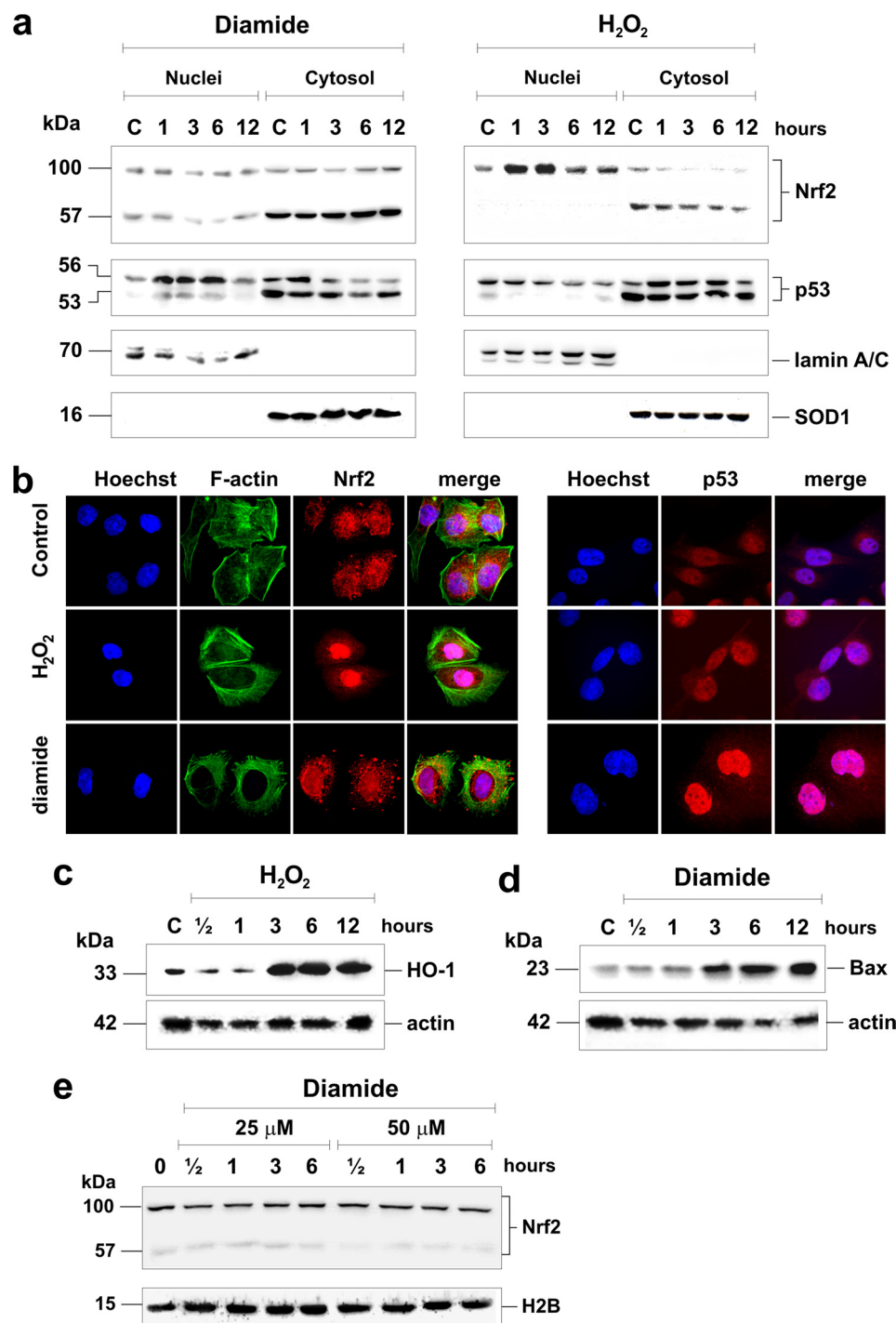
FIGURE 5. **H₂O₂ and diamide specifically modulate Nrf2 or p53 in AGS cells.** AGS cells were treated with 200 μM H₂O₂ or diamide for 1 h and transferred to fresh medium. *a*, at the indicated times of recovery, nuclear- and cytosol-enriched fractions were purified. Twenty micrograms of cytosolic and nuclear cell extracts were loaded for detection of p53 and Nrf2 levels. Copper,zinc superoxide dismutase (*SOD1*) and lamin A/C were used as cytosolic and nuclear loading control (*lanes C*), respectively. Immunoblots are from one experiment representative of three that gave similar results. *b*, after 3 h of recovery, cells were fixed with *p*-formaldehyde and subjected to immunostaining with an anti-Nrf2 (*red, left panel*) or an anti-p53 antibody (*red, right panel*) and fluorescein isothiocyanate-conjugated phalloidin (*green, left panel*). Nuclei (*blue*) were stained with Hoechst 33342. Images reported are from one experiment of three that gave similar results. *c*, at the indicated times of recovery, cells were lysed. Thirty micrograms of total cell extracts were loaded for detection of heme oxygenase-1 (*HO-1*) levels. Actin was used as loading control. Immunoblots are from one experiment representative of three that gave similar results. *d*, at the indicated times of recovery, cells were lysed. Thirty micrograms of total cell extracts were loaded for detection of Bax levels. Actin was used as loading control. Immunoblots are from one experiment representative of three that gave similar results. *e*, AGS cells were treated with 25 or 50 μM diamide for 1 h and transferred to fresh medium. At the indicated times of recovery, nuclear-enriched fractions were purified. Twenty micrograms of nuclear extracts were loaded for detection of Nrf2 levels. Histone H2B was used as nuclear loading control. Immunoblots are from one experiment representative of three that gave similar results.

whereas diamide was able to induce an early dramatic accumulation of the protein within the nucleus. To confirm that nuclear localization of p53 and Nrf2 was followed by the acquisition of their transcriptional properties, we analyzed the expression levels of Bax and heme oxygenase-1 that are specifically expressed downstream of p53 or Nrf2, respectively. Fig. 5, *c* and *d*, shows Western blot analyses of these proteins in total cell lysates. The immunoblots indicate a significant increase of their expression levels starting from 3 h after the removal of the respective oxidative inducer. These data correlate nicely with those obtained previously by Western blotting and immunofluorescence and corroborate the hypothesis that each treatment preferentially activates a specific pathway. However, the observed differences could be due either to the strength of the signal or to qualitative divergence in the activation of the two pathways. We therefore treated the cells with sublethal doses of diamide and evaluated whether Nrf2 was activated. Western blot analysis of nuclear fraction reveals that no significant nuclear accumulation of the transcription factor was evidenced upon treatment with 25 or 50 μM diamide (Fig. 5*e*), confirming the unresponsiveness of Nrf2 to diamide.

Inhibition of p53 or Nrf2 Reverses Cell Response—To evaluate the role of p53 in apoptosis, we transfected AGS cells with an siRNA against p53 (sip53 cells). Western blot analysis of p53 indicated that the concentration of the protein decreased rapidly after transfection (Fig. 6*a*). In the light of this result, we treated the cells with diamide 12 h after transfection. Cytofluorometric analyses showed that the extent of apoptosis decreased significantly (about 35%) in sip53 (Fig. 6*b*). Moreover, we transfected AGS cells with DN-Nrf2 (6) fused with green fluorescent protein. The efficiency of transfection was estimated to be about 80% (Fig. 6*c*) as assayed by immunofluorescence. Data reported
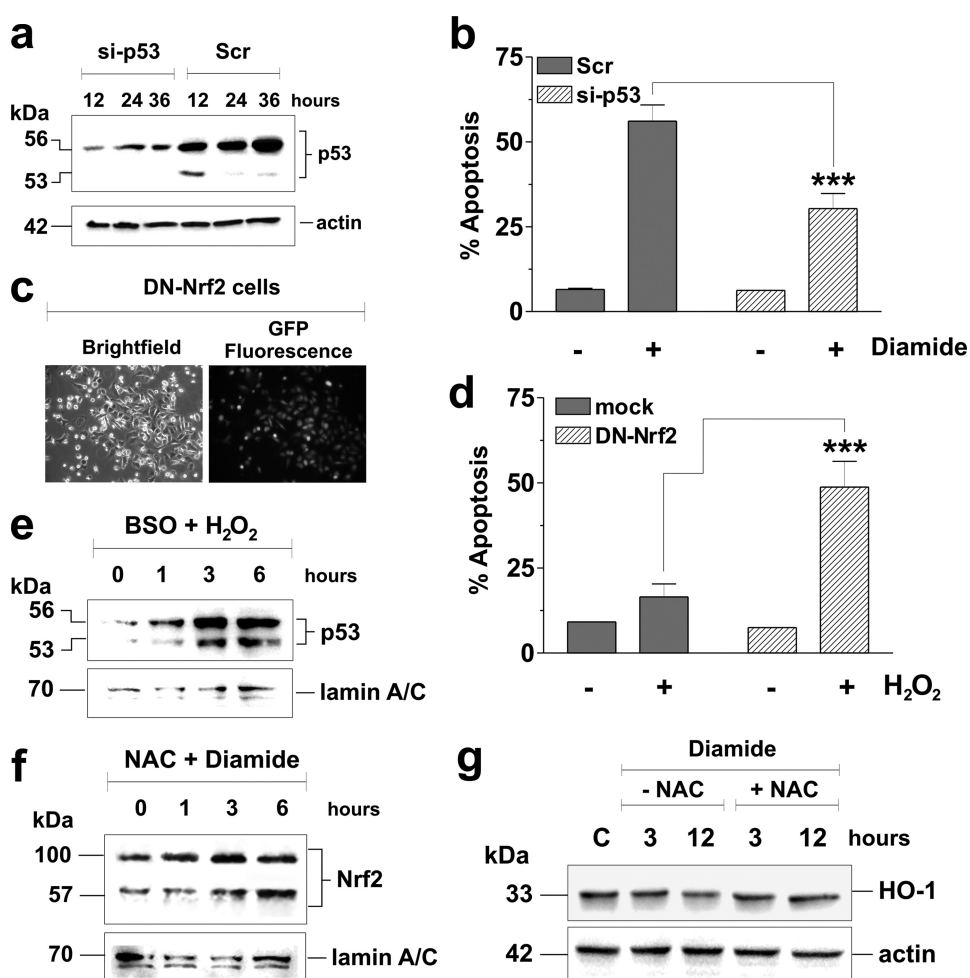
a

si-p53   Scr

kDa   12 24 36   12 24 36   hours

56 —

53 — p53

42 — actin

b

c   DN-Nrf2 cells

Brightfield   GFP Fluorescence

d

e   BSO + H$_2$O$_2$

kDa   0   1   3   6   hours

56 —

53 — p53

70 — lamin A/C

f   NAC + Diamide

kDa   0   1   3   6   hours

100 —

57 — Nrf2

70 — lamin A/C

g   Diamide

- NAC   + NAC

kDa   C   3 12   3 12   hours

33 — HO-1

42 — actin

FIGURE 6. **Inhibition of Nrf2 or p53 reverses cell response.** *a*, AGS cells were transfected with a siRNA against p53 (si-p53 cells) or with a scramble sequence (Scr). Twelve hours after transfection, si-p53 and Scr cells were treated with 200 μM diamide for the indicated times. Twenty micrograms of total cell extracts were loaded after transfection for detection of p53 protein levels. Actin was used as loading control. Immunoblots are from one experiment representative of five that gave similar results. *b*, 12 h after transfection, si-p53 and Scr cells were treated with 200 μM diamide. After 1 h of recovery, cells were transferred to fresh medium, cultured for an additional 12 h, and finally stained with propidium iodide for cytofluorometric analyses of apoptosis. Data are expressed as means ± S.D. (*n* = 5). ***, *p* < 0.001. *c*, AGS cells were transfected with DN-Nrf2 cDNA. Forty-eight hours after transfection, green fluorescent protein (*GFP*) fluorescence was visualized to monitor transfection efficiency. *d*, AGS cells were transfected with DN-Nrf2 cDNA and control vector (*mock*). Forty-eight hours after transfection, cells were treated for 1 h with 200 μM H$_2$O$_2$, transferred to fresh medium, cultured for additional 24 h, and stained with propidium iodide for cytofluorometric analyses of apoptosis. Data are expressed as means ± S.D. (*n* = 5). ***, *p* < 0.001. *e*, AGS cells were incubated with 1 mM BSO for 12 h and then treated with 200 μM H$_2$O$_2$. After 1 h of treatment, cells were transferred to fresh medium containing 1 mM BSO and cultured further. At the indicated times of recovery, nuclei were purified. Twenty micrograms of nuclear cell extract were loaded for detection of Nrf2 protein levels. Lamin A/C was used as loading control. *f*, AGS cells were incubated with 5 mM CysNAc (*NAC*) for 1 h and then treated with 200 μM diamide. After 1 h of treatment, cells were transferred to fresh medium containing 5 mM CysNAc and cultured further. At the indicated times of recovery, nuclei were purified. Twenty micrograms of nuclear cell extract were loaded for detection of Nrf2 protein levels. Lamin A/C was used as loading control. Immunoblots are from one experiment representative of three that gave similar results. *g*, alternatively, after 3 and 12 h, cells were lysed. Thirty micrograms of total cell extracts were loaded for detection of heme oxygenase-1 (*HO-1*) levels. Actin was used as loading control. Immunoblots are from one experiment representative of three that gave similar results.

6*f*). However, no increase in the heme oxygenase-1 immunoreactive band was detected, implying that Nrf2 transcriptional activity was not induced (Fig. 6*g*).

Mechanistic Insight into the Different Response of AGS Cells to Pro-oxidants—To unravel the redox bases underlying the different response of Nrf2 to H$_2$O$_2$ and diamide, we looked at Keap1. Under physiological conditions, Keap1 acts as a repressor of Nrf2 activity both by direct interaction and subsequent Nrf2 sequestration into the cytoplasm and by controlling Nrf2 stability/degradation. Oxidation of two conserved Keap1 cysteines (Cys[273] and Cys[288]) seems to be involved in the regulation of these events (12). We therefore estimated Keap1 oxidation state by redox Western blotting upon incubation with AMS. AGS cells were treated with 200 μM H$_2$O$_2$ or diamide and recovered at 1 and 3 h. Protein lysates were incubated with AMS to distinguish free from oxidized sulfydryls. Fig. 7*a* shows the appearance of a low molecular mass (oxidized) band of Keap1 already after 1 h of treatment with H$_2$O$_2$, which declined to control (reduced) values after 3 h. On the contrary, no shift was observed in diamide-treated cells, indicating the specific oxidation of Keap1 only in response to H$_2$O$_2$. These results indicate that a redox-sensitive component governing diamide-induced cell death should also exist. We identified Trx1 as a possible player because of its high reactivity toward diamide with respect to other thiol-containing proteins. For this reason, we treated AGS cells with 200 μM H$_2$O$_2$ or diamide and followed the redox state of Trx1 by redox Western blotting on urea-PAGE. This method

in Fig. 6*d* show that the percentage of apoptosis of DN-Nrf2 cells increased significantly (about 3-fold) with respect to AGS carrying the empty vector. Next, we evaluated whether BSO- and CysNAc-mediated effects were associated with the modulation of Nrf2 and p53. To this aim, AGS cells were incubated with 1 mM BSO and then treated with 200 μM H$_2$O$_2$. Fig. 6*e* shows that p53, under GSH depletion, accumulated rapidly within the nuclear compartment. Cells incubated with 5 mM CysNAc before diamide treatment showed only a modest increase of Nrf2 levels in the nucleus (Fig.

allows separation of Trx1 redox forms and evaluation of the occurrence of oxidation reactions on cysteine residues. Fig. 7*b* shows that H$_2$O$_2$ did not induce changes in the ratio between oxidized and reduced Trx1, whereas an increase in the intensity of the immunoreactive bands was detected at 6 and 12 h. Conversely, as early as 30 min after diamide removal, the ratio between reduced and oxidized Trx1 increased to values of about 1, confirming that Trx1 had been specifically oxidized under diamide treatment (Fig. 7*b*). To validate further the spec-
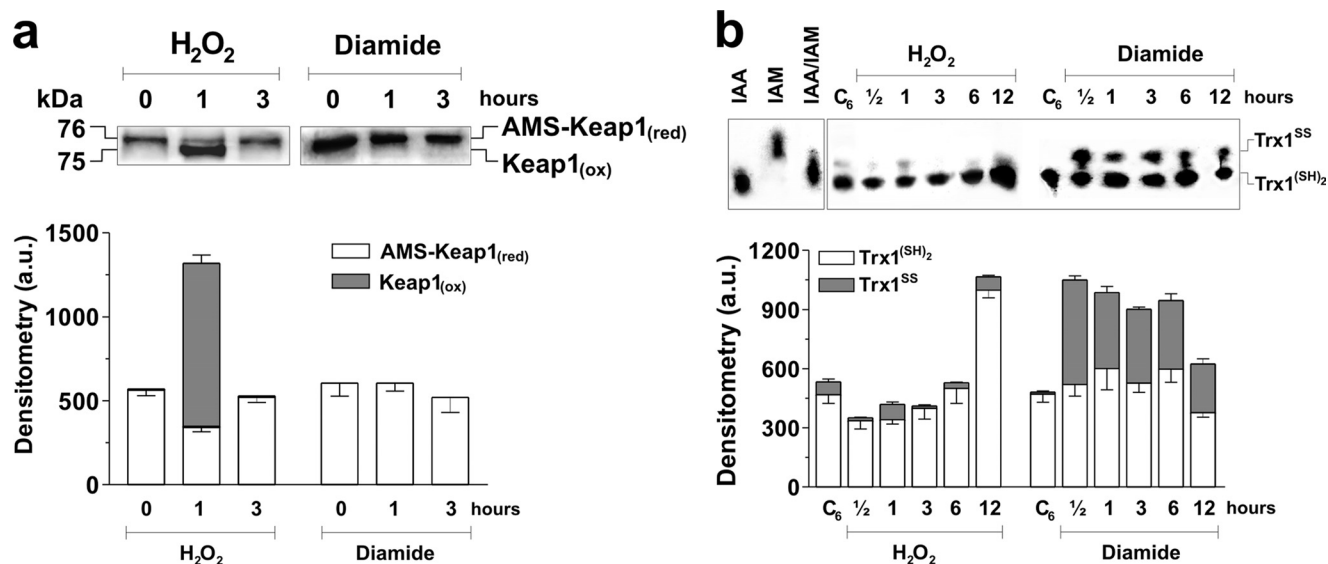
FIGURE 7. **Redox switches of H₂O₂- or diamide-mediated pathways.** AGS cells were treated with 200 μM H₂O₂ or diamide and transferred to fresh medium. *a*, at the indicated times of recovery, cells were precipitated in trichloroacetic acid and dissolved in 20 mM Tris/HCl (pH 8.0) containing AMS to allow modifying free thiols. Keap1 redox forms were then separated on 7.5% SDS-PAGE in nonreducing conditions. On the *right*, reduced (AMS-bound) Keap1 (*AMS-Keap1*(red)) and oxidized Keap1 (*Keap1*(ox)) are shown. Density of reduced (AMS-Keap1) and oxidized (Keap1) (reported below the immunoblots) was calculated using the software Quantity One and is reported as arbitrary units (*a.u.*). Data are expressed as means ± S.D. ($n = 3$). *b*, at the indicated times of recovery, cell were lysed in urea buffer, and samples were treated with iodoacetic acid (*IAA*) to obtain the carboxymethylation of sulfydryl groups, and the subsequent amidomethylation of thiols previously engaged in disulfides with iodoacetamide (*IAM*). Proteins were separated on a 9% urea-polyacrylamide gel for monitoring Trx1 redox status. Immunoblots are from one experiment representative of three that gave similar results. On the *right*, controls of fully reduced (*IAA*), fully oxidized (*IAM*), or partially oxidized (*IAA/IAM*) Trx1 are shown. Density of reduced (*Trx$^{SH}_2$*) and oxidized (*Trx^{SS}*) Trx1 (reported below the immunoblots) is reported as arbitrary units. Data are expressed as means ± S.D. ($n = 3$).

ificity of the pathways activated by H₂O₂ and diamide, we evaluated whether Keap1 could be oxidized upon treatment with doses of diamide unable to induce cell death (25 and 50 μM). No band shift was observed under these conditions. However, oxidation of Trx1 was not detected (data not shown), even after treatment of cells with 1 mM H₂O₂, a condition that resulted in extensive cell death (about 50%).

Trx1 Oxidation Correlates with p38^{MAPK}-dependent Phosphorylation of p53—It is well established that Trx1 functions as the inhibitory subunit of ASK1, the MAPK kinase kinase upstream of JNK and p38^{MAPK}. To elucidate which member of MAPK was activated in response to diamide, we followed, by Western blotting, the phospho-active levels of JNK and p38^{MAPK}. Fig. 8*a* shows that p38^{MAPK} was activated rapidly at 30 min of recovery from diamide removal, whereas the levels of phospho-JNK remained unaltered throughout the experimental times. Other experiments performed in the presence of the specific inhibitors of JNK and p38^{MAPK}, SP600125 and SB203580, respectively, confirmed these results. Fig. 8*b* shows that a significant decrease in the extent of apoptotic cells occurred only upon p38^{MAPK} inhibition, whereas no protection was achieved by inhibiting JNK-mediated signaling. We also determined the phosphorylation state of p38^{MAPK} upon treatment with 1 mM H₂O₂, and no increase of phospho-p38^{MAPK} was observed after 3 h (Fig. 8*c*), confirming that AGS cells did not activate Trx1/p38^{MAPK}-mediated apoptosis under H₂O₂ challenge.

To define the specific contribution of p38^{MAPK} and p53 and their possible cross-talk in the induction of apoptosis in response to diamide, we treated AGS cells with 200 μM diamide in the presence of SB203580, and we monitored by fluorescence

microscopy the activation of p53 after 3 h of recovery. As expected, p38^{MAPK} and p53 were found to be activated within 1 h of treatment. In particular, images depicted in Fig. 8*d* show that both proteins accumulated within the nuclear compartment upon exposure to diamide and that the inhibition of p38^{MAPK} correlated nicely with a strong decrease in p53 activation and nuclear localization. Moreover, Fig. 8*e* shows Western blot analyses of p53 in the presence of the p38^{MAPK} inhibitor. A 3-fold decrease of p53 expression levels was determined, confirming the positive regulation by p38^{MAPK} of p53 in response to diamide. To confirm these results, we transfected AGS cells with an siRNA against p38^{MAPK} (sip38^{MAPK} cells) and treated them with diamide for 24 h. Cytofluorometric analyses showed that the extent of apoptosis decreased as much as observed previously upon incubation with SB203580 (Fig. 8*f*). Moreover, Western blot analyses of sip38^{MAPK} cells indicated that the p38^{MAPK}/p53 apoptotic axis was not activated after 3- and 6-h treatment with diamide. Indeed, in sip38^{MAPK} cells, the expression levels of these proteins and Bax remained at levels comparable with those of the control (Fig. 8*g*).

Effects of H₂O₂ and Diamide on CaCo2 Cells—To confirm and generalize the results obtained in AGS cells, we selected another adenocarcinoma cell line, CaCo2, which has been reported to express GI-glutathione peroxidase (27, 28). However, in contrast to AGS, these cells express a truncated/null form of p53 (29). CaCo2 cells were treated with 200 μM H₂O₂ for 1 h and monitored after different times of recovery. Data in Fig. 9 show that 24-h treatment with H₂O₂ induced cell cycle arrest in G₂/M phase without any significant increase in the extent of sub-G₁. This response correlated well with the glutathione concentrations measured. In particular, Fig. 9*a* shows
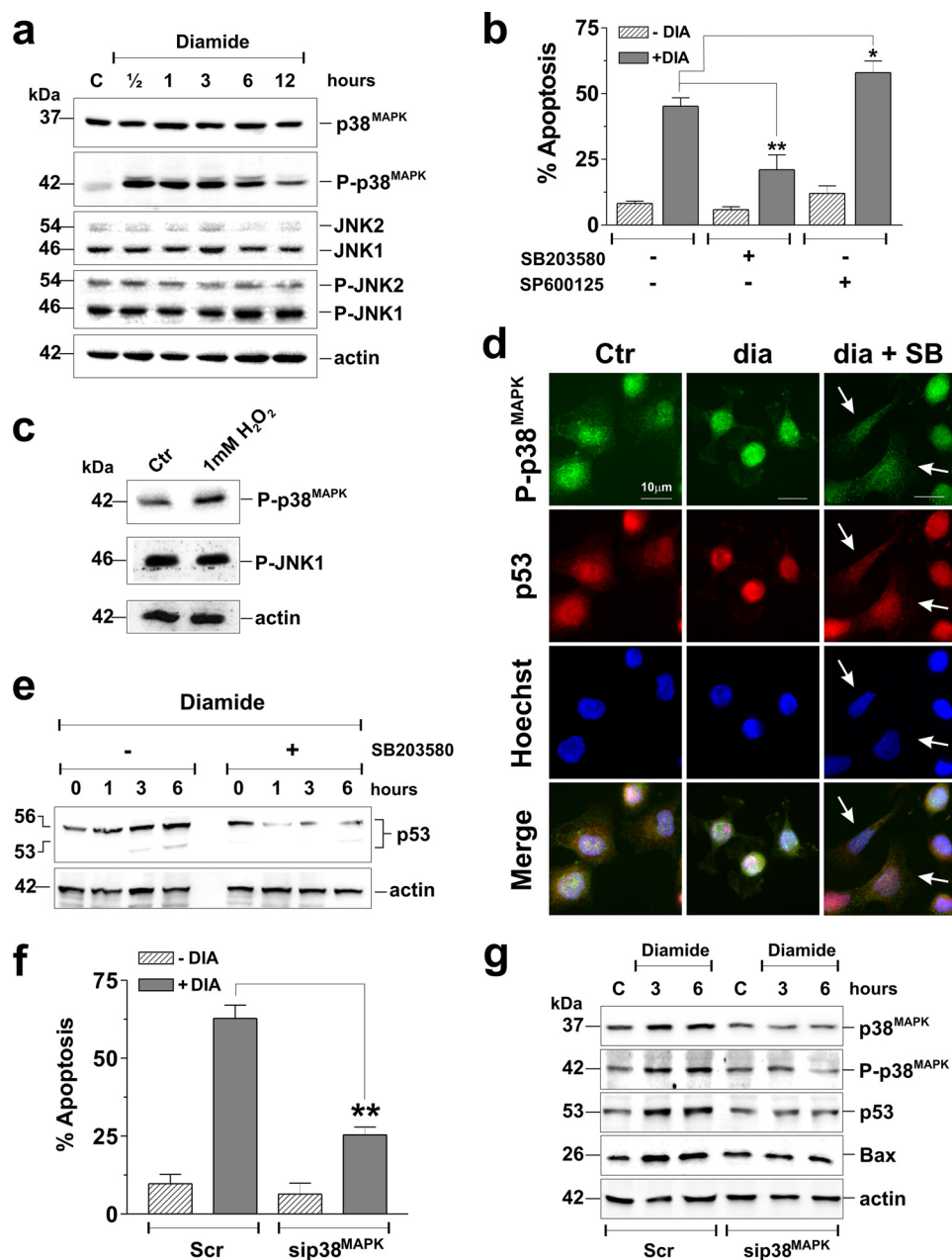
FIGURE 8. **Trx1 oxidation correlates to p38^{MAPK}-dependent phosphorylation of p53.** *a*, AGS cells were treated with 200 μM diamide for 1 h and transferred to fresh medium. At the indicated times of recovery, cells were lysed. Thirty micrograms of total cell extracts were loaded for detection of the basal and phospho-activated levels of p38^{MAPK} and JNK. Actin was used as loading control. Immunoblots are from one experiment representative of three that gave similar results. *b*, AGS cells were incubated with 10 μM SP600125 or 15 μM SB203580 for 1 h and then treated with 200 μM diamide. After 1 h, cells were transferred to fresh medium containing the inhibitors, cultured for an additional 24 h, and stained with propidium iodide for cytofluorometric analysis of apoptosis. Data are expressed as means ± S.D. ($n = 5$). *, $p < 0.05$; **, $p < 0.01$. *c*, AGS cells were treated with 1 mM H$_2$O$_2$ for 1 h and transferred to fresh medium. After 3 h of recovery, cells were lysed. Thirty micrograms of total cell extracts were loaded for detection of the basal and phospho-activated levels of p38^{MAPK} and JNK. Actin was used as loading control. Immunoblots are from one experiment representative of three that gave similar results. *d*, AGS cells were incubated with 15 μM SB203580 for 1 h and then treated with 200 μM diamide. After 1 h of treatment, cells were transferred to fresh medium containing the inhibitor, cultured for an additional 3 h, fixed with *p*-formaldehyde, and subjected to immunostaining with an anti-p53 antibody (*red*) or an anti-phospho-p38^{MAPK} (*green*). Nuclei (*blue*) were stained with Hoechst 33342. Images reported are from one experiment of three that gave similar results. *e*, Alternatively, after 1, 3, and 6 h, cells were lysed. Twenty micrograms of total cell extracts were loaded for detection of p53 levels. Actin was used as loading control. Immunoblots are from one experiment representative of three that gave similar results. *f*, AGS cells were transfected with a siRNA against p38^{MAPK} (sip38^{MAPK} cells) or with a scramble sequence (Scr). Twelve hours after transfection, sip38^{MAPK} and Scr cells were treated with 200 μM diamide. After 1 h of recovery, cells were transferred to fresh medium, cultured for an additional 24 h, and finally stained with propidium iodide for cytofluorometric analyses of apoptosis. Data are expressed as means ± S.D. ($n = 3$). **, $p < 0.01$. *g*, alternatively, 20 μg of total cell extracts were loaded after transfection for the detection of basal and phospho-activated p38^{MAPK}, p53, and Bax. Actin was used as loading control. Immunoblots are from one experiment representative of three that gave similar results.

that, similar to AGS, CaCo2 cells responded to H$_2$O$_2$ by an early increase of GS-R content (3–6 h) followed by a late rise of GSH (12–24 h). At the same time, no detectable modulation of GSSG was observed. We also performed fluorescence microscopy analysis of Nrf2 localization in CaCo2 cells upon 3-h recovery with H$_2$O$_2$ or diamide. Fig. 9*b* shows significant nuclear accumulation of Nrf2 upon treatment with H$_2$O$_2$. On the contrary, no change was observed upon treatment with diamide, confirming the H$_2$O$_2$-selective activation of Nrf2.

Because of the absence of a functional p53, the use of CaCo2 cells allowed an evaluation of the role of p53 in diamide-induced toxicity. As expected, CaCo2 cells did not undergo apoptosis upon diamide treatment (Table 2). However, Western blot analyses of phospho-p38^{MAPK} evidenced a rapid increase of the immunoreactive band of the protein within 1 h of treatment, which was maintained throughout the experimental time (Fig. 9*c*). These results indicated that p38^{MAPK} was activated in CaCo2 cells, but the absence of a functional p53 did not allow the signal being transduced into an apoptotic response. To confirm this assumption, we transfected CaCo2 cells with a pcDNA3 vector expressing the WT form of p53 (WTp53 cells, see *inset* of Fig. 9*d*) and monitored cell response to diamide. Cytofluorometric analysis (Fig. 9*d*) showed that the number of apoptotic cells increased significantly under these experimental conditions, confirming that p53 governs the apoptotic response to diamide.

DISCUSSION

Resistance of some tumor histotypes, such as gastric and intestine carcinomas, to apoptosis induced by ROS-generating chemotherapeutics has been reported to depend in part on the high expression of detoxifying and antioxidant enzymes, among which GI-glutathione peroxidase should be men-
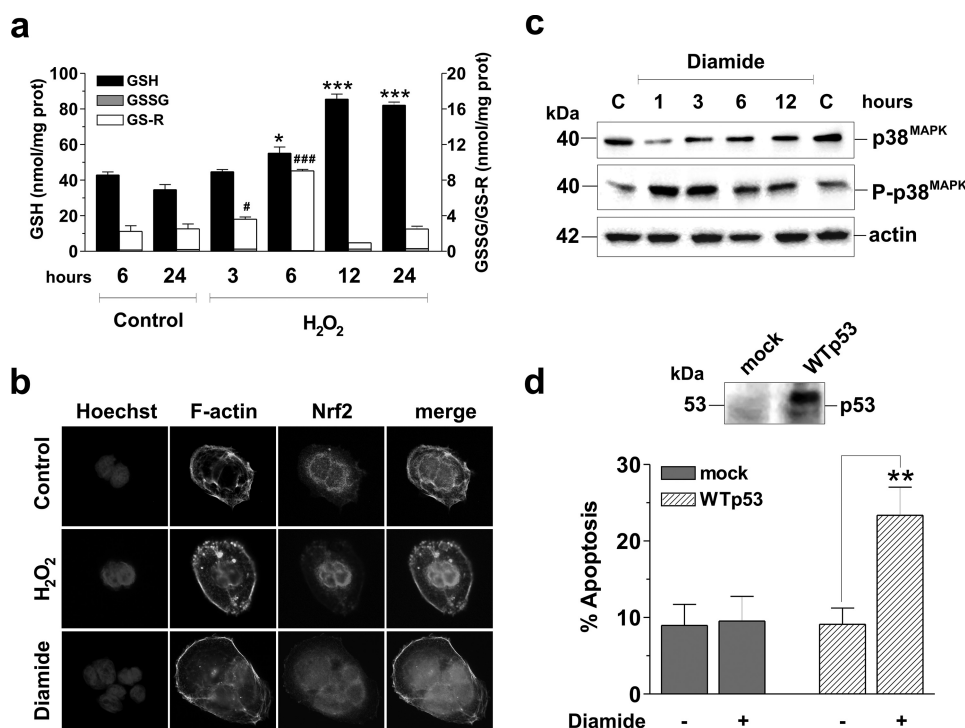
FIGURE 9. **Effects of diamide or H_2O_2 on CaCo2 cells.** *a*, CaCo2 cells were treated with 200 μM H_2O_2 for 1 h and transferred to fresh medium. At the indicated times of recovery, cells were collected, washed exhaustively with phosphate-buffered saline, and used for GSH, GSSG, and GS-R assay by HPLC, as described under "Experimental Procedures." GSH, GSSG, and GS-R data are expressed as nanomoles/mg of total protein. Values represent means ± S.D. (*n* = 5). For GSH: *, $p < 0.05$; ***, $p < 0.001$. For GS-R: #, $p < 0.05$; ###, $p < 0.001$. *b*, CaCo2 cells were treated with 200 μM H_2O_2 or diamide for 1 h and transferred to fresh medium. After 3 h of recovery, cells were fixed with *p*-formaldehyde and subjected to immunostaining with an anti-Nrf2 (*red*) and fluorescein isothiocyanate-conjugated phalloidin (*green*). Nuclei (*blue*) were stained with Hoechst 33342. Images reported are from one experiment of three that gave similar results. *c*, CaCo2 cells were treated with 200 μM diamide for 1 h and transferred to fresh medium. At the indicated times of recovery, cells were lysed. Thirty micrograms of total cell extracts were loaded for detection of the basal and phospho-activated levels of p38^{MAPK}. Actin was used as loading control. Immunoblots are from one experiment representative of three that gave similar results. *d*, CaCo2 cells were transfected with WTp53 cDNA or control vector (*mock*). Twenty-four hours after transfection, cells were treated for 1 h with 200 μM diamide, transferred to fresh medium, cultured for additional 24 h, and stained with propidium iodide for cytofluorometric analysis of apoptosis. Data are expressed as means ± S.D. (*n* = 5). **, $p < 0.01$.

TABLE 2
Cell cycle distribution of CaCo2

CaCo2 cells were plated at a density of $2 \times 10^4/cm^2$ and treated with 200 mM hydrogen peroxide and diamide for 1 h. Cells were then transferred to fresh medium for 24 h, washed, and stained with propidium iodide. Analysis of cell cycle and apoptosis was performed by a FACScalibur instrument, and percentages of positive-staining cells were calculated using WinMDI version 2.8 software. Values reported represent the mean ± S.D. of *n* = 5 independent experiments.

Treatment	Sub-G_1	G_2/M
	% of population	
Control	9.9 ± 1.4	22.1 ± 3.6
H_2O_2	8.5 ± 2.0	60.2 ± 3.7
Diamide	9.2 ± 1.8	26.4 ± 2.5

dramatically increased GSSG levels and completely cleared the GS-R content. However, after diamide treatment, the amount of GSH also increased significantly, indicating a rapid activation of GSH neosynthesis and/or a release from the aliquot engaged in GS-R. By combining these results and considering the high glutathione peroxidase activity present in AGS cells, it is conceivable that GSH counters H_2O_2 challenge by functioning as a cofactor of glutathione peroxidase and by inhibiting irreversible oxidation of protein thiols. Instead, diamide could induce the release of protein-bound GSH, thus reasonably mediating further cysteine oxidation of specific diamide-sensitive proteins, such as dithiol-containing proteins.

It has been demonstrated that, under oxidative conditions, the vicinal thiols of Trx1 undergo disulfide bridge formation, thus leading ASK1 free to be activated by autophosphorylation. This mechanism probably underlies the induction of the downstream p38^{MAPK}-dependent apoptotic signaling cascade, eventually culminating in the activation of the mitochondrial pathway (22, 30). Here, we identified Trx1 as the protein regulated by diamide. We also defined the involvement of p38^{MAPK} in the activation of p53 and p53-related apoptotic events. In fact, both chemical and post-transcriptional inhibition of p38^{MAPK} prevented p53 activation and Bax up-regulation and apoptosis in AGS cells. Moreover, the expression of p53 in CaCo2 cells made it possible to induce apoptosis by diamide also in this cell line. Therefore, we suggest that the Trx1/p38^{MAPK}/p53 signaling axis is the apoptotic pathway operative upon disulfide stress. This result is in agreement with data from the literature that indicate that p38^{MAPK} is the p53 upstream kinase responsible for the induction of apoptosis upon different stimuli, such as mechanical stress-induced DNA damage (31), human immunodeficiency virus infection (32, 33), treatment with 6-hydroxydopamine (34), and UV exposure (35). Whether the relationship between p38^{MAPK} and p53 is direct or mediated by other proteins, such as p18^{Hamlet} (36), is beyond the scope of this work. However, it represents an issue that deserves to be investigated further in the future to define completely the AGS cell response to proapoptotic redox stressors.

In this work we also identified the redox sensor responsible for H_2O_2 resistance in carcinoma cells. We demonstrated that Nrf2 mediates the antioxidant/survival response to H_2O_2 in a Keap1-dependent manner. Indeed, Keap1 represents the redox

tioned (17, 28). In line with these findings, we report here that the gastric cell line AGS is resistant to H_2O_2 and other ROS producers, such as paraquat and xanthine/xanthine oxidase. We also demonstrate that ROS resistance can be circumvented by inducing oxidative unbalance with thiol-oxidizing compounds, such as DTNB and diamide, which efficiently induced apoptosis via an intrinsic pathway (release of cytochrome *c* and activation of caspase-9 and caspase-3). In this experimental system, H_2O_2 yields a transient increase of intracellular GSH and GS-R without affecting the GSSG content, whereas diamide

switch for Nrf2 activation (12, 37). Although Nrf2 is the final effector, Keap1 represents the real inducer of the antioxidant response, indicating for the Nrf2/Keap1 heterodimer a characteristic two-module redox-sensitive system. By redox Western blot analyses we demonstrated that Keap1 undergoes cysteine oxidation only upon treatment with H_2O_2, whereas diamide never affects its oxidation state. This result correlates nicely with microscopic analyses of Nrf2 localization and the expression of Nrf2 gene target heme oxygenase-1, which occurs only in response to H_2O_2.

Although both H_2O_2 and diamide are two-electron oxidants, they react differently with cellular components. In particular, H_2O_2 easily oxidizes GSH and phospholipids, as well as DNA and proteins, with the diffusion rate and the concentration of targets being the principal limiting step regulating its reactivity. On the contrary, diamide specifically oxidizes cellular sulfydryls, mainly GSH and a few reactive proteins, such as Trx1. This suggests that the cellular antioxidant system and the availability of free GSH modulate cell response. This assumption is also strengthened by other results, such as: (i) the similarity of response to oxidants belonging to the same class of compounds (disulfides *versus* ROS producers); (ii) the unresponsiveness of Nrf2 to low/nonapoptotic doses of diamide; (iii) the absence of Keap1 oxidation upon diamide treatment; (iv) the absence of Trx1 oxidation upon H_2O_2 treatment, even at concentrations that efficiently result in cell death; (v) the reproducibility of the results obtained with CaCo2 cells. Altogether, the data indicate that in ROS-resistant cells, such as carcinoma cells, diamide does not activate the Keap1/Nrf2 pathway and Nrf2-mediated survival, even when cells do not undergo apoptosis. It should also be remembered that GI-glutathione peroxidase is transcriptionally regulated by Nrf2 (28), suggesting the presence of a positive GI-glutathione peroxidase/Nrf2 loop necessary for protection against H_2O_2.

It is now well established that the up-regulation of antioxidant enzymes and the activation of transcription factors mediating survival signals are an adaptation response to counteract oxidative stress, such as that induced by anticancer drugs. Identification of the molecular players involved in this phenomenon could be useful or even necessary to improve therapeutic strategies (38). For example, recent work demonstrates that resistance of murine embryonic fibroblasts to BSO treatment can be circumvented in Nrf2-deficient cells (39), indicating that the abrogation of Nrf2 activity in combination with GSH depletion is a possible chemotherapeutic approach. The therapeutic efficacy of a combination between the inhibition of the anti-apoptotic protein Bcl2 and treatment with the synthetic pro-oxidant retinoid *N*-(4-hydroxyphenyl)retinamide in leukemia cells has been also evaluated (40). Based on such observations, many ROS-generating agents are currently in clinical trials as single agents or in combination (*e.g.* the combined use of the GSH-depleting agent imexon or the iron-chelator Triapine® with the chemotherapeutics gemcitabine or docetaxel) (41). In this scenario, our results add a fundamental contribution to the comprehension of the molecular mechanisms underlying cell responses to oxidative stress. In particular, we provide evidence that in ROS-resistant cells the activation of p53-dependent apo-

ptosis or of the Nrf2-mediated resistance is principally responsive to the type of oxidative stress, *i.e.* disulfides *versus* ROS, and not to its extent. This means that both the cell antioxidant defense and the redox chemistry of an anticancer drug should be characterized early to design appropriate therapies against different types of cancer cells.

REFERENCES

1. Behrend, L., Henderson, G., and Zwacka, R. M. (2003) *Biochem. Soc. Trans.* **31,** 1441–1444
2. Pelicano, H., Carney, D., and Huang, P. (2004) *Drug Res. Updat.* **7,** 97–110
3. Rotilio, G., Mavelli, I., Rossi, L., and Ciriolo, M. R. (1985) *Environ. Health Perspect.* **64,** 259–264
4. Filomeni, G., Rotilio, G., and Ciriolo, M. R. (2005) *Cell Death Differ.* **12,** 1555–1563
5. Arnér, E. S., and Holmgren, A. (2006) *Semin. Cancer Biol.* **16,** 420–426
6. Liu, Y., and Min, W. (2002) *Circ. Res.* **90,** 1259–1266
7. Adler, V., Yin, Z., Tew, K. D., and Ronai, Z. (1999) *Oncogene* **18,** 6104–6411
8. Na, H. K., and Surh, Y. J. (2006) *Mol. Carcinog.* **45,** 368–380
9. Kim, Y. C., Yamaguchi, Y., Kondo, N., Masutani, H., and Yodoi, J. (2003) *Oncogene* **22,** 1860–1865
10. Chen, C., and Kong, A. N. (2004) *Free Radic. Biol. Med.* **36,** 1505–1516
11. Chen, C., Pung, D., Leong, V., Hebbar, V., Shen, G., Nair, S., Li, W., and Kong A. N. (2004) *Free Radic. Biol. Med.* **37,** 1578–1590
12. Kensler, T. W., Wakabayashi, N., and Biswal, S. (2007) *Annu. Rev. Pharmacol. Toxicol.* **47,** 89–116
13. Riley, T., Sontag, E., Chen, P., and Levine, A. (2008) *Nat. Rev. Mol. Cell Biol.* **9,** 402–412
14. Rainwater, R., Parks, D., Anderson, M. E., Tegtmeyer, P., and Mann, K. (1995) *Mol. Cell. Biol.* **15,** 3892–3903
15. Seemann, S., and Hainaut, P. (2005) *Oncogene* **24,** 3853–3863
16. Faraonio, R., Vergara, P., Di Marzo, D., Pierantoni, M. G., Napolitano, M., Russo, T., and Cimino, F. (2006) *J. Biol. Chem.* **281,** 39776–39784
17. Filomeni, G., Aquilano, K., Rotilio, G., and Ciriolo, M. R. (2005) *Cancer Res.* **65,** 11735–11742
18. Nicoletti, I., Migliorati, G., Pagliacci, M. C., Grignani, F., and Riccardi, C. (1991) *J. Immunol. Methods* **139,** 271–279
19. Filomeni, G., Cerchiaro, G., Da Costa Ferriera, A. M., De Martino, A., Pedersen, J. Z., Rotilio, G., and Ciriolo, M. R. (2007) *J. Biol. Chem.* **282,** 12010–12021
20. Halvey, P. J., Watson, W. H., Hansen, J. M., Go, Y. M., Samali, A., and Jones, D. P. (2005) *Biochem. J.* **386,** 215–219
21. Bersani, N. A., Merwin, J. R., Lopez, N. I., Pearson, G. D., and Merrill, G. F. (2002) *Methods Enzymol.* **347,** 317–326
22. Filomeni, G., Rotilio, G., and Ciriolo, M. R. (2003) *FASEB J.* **17,** 64–66
23. Lowry, O. H., Rosebrough, N. J., Farr, A. L., and Randall, R. J. (1951) *J. Biol. Chem.* **193,** 265–275
24. Xu, W., Liu, L., Smith, G. C., and Charles, G. (2000) *Nat. Cell Biol.* **2,** 339–345
25. Han, Z., Malik, N., Carter, T., Reeves, W. H., Wyche, J. H., and Hendrickson, E. A. (1996) *J. Biol. Chem.* **271,** 25035–25040
26. Kang, K. W., Lee, S. J., Park, J. W., and Kim, S. G. (2002) *Mol. Pharmacol.* **62,** 1001–1010
27. Wingler, K., Müller, C., Shmehel, K., Florian, S., and Brigelius-Flohé, R. (2000) *Gastroenterology* **119,** 420–430
28. Banning, A., Deubel, S., Kluth, D., Zhou, Z., and Brigelius-Flohé, R. (2005) *Mol. Cell. Biol.* **25,** 4914–4923
29. Djelloul, S., Forgue-Lafitte, M.-E., Hermelin, B., Mareel, M., Bruyneel, E., Baldi, A., Giordano, A., Chastre, E., and Gespach, C. (1997) *FEBS Lett.* **406,**

234–242

30. Saitoh, M., Nishitoh, H., Fujii, M., Takeda, K., Tobiume, K., Sawada, Y., Kawabata, M., Miyazono, K., and Ichijo, H. (1998) *EMBO J.* **17,** 2596–2606

31. Mayr, M., Hu, Y., Hainaut, H., and Xu, Q. (2002) *FASEB J.* **16,** 1423–1425

32. Perfettini, J. L., Castedo, M., Nardacci, R., Ciccosanti, F., Boya, P., Roumier, T., Larochette, N., Piacentini, M., and Kroemer, G. (2005) *J. Exp. Med.* **201,** 279–289

33. Perfettini, J. L., Nardacci, R., Bourouba, M., Subra, F., Gros, L., Séror, C., Manic, G., Rosselli, F., Amendola, A., Masdehors, P., Chessa, L., Novelli, G., Ojcius, D. M., Siwicki, J. K., Chechlinska, M., Auclair, C., Regueiro, J. R., de Thé, H., Gougeon, M. L., Piacentini, M., and Kroemer, G. (2008) *PLoS ONE* **3,** e2458

34. Gomez-Lazaro, M., Galindo, M. F., Concannon, C. G., Segura, M. F., Fernandez-Gomez, F. J., Llecha, N., Comella, J. X., Prehn, J. H., and Jordan, J.

(2008) *J. Neurochem.* **104,** 1599–1612

35. Hildesheim, J., Bulavin, D. V., Anver, M. R., Alvord, W. G., Hollander, M. C., Vardanian, L., and Fornace, A. J., Jr. (2002) *Cancer Res.* **62,** 7305–7315

36. Cuadrado, A., Lafarga, V., Cheung, P. C., Dolado, I., Llanos, S., Cohen, P., and Nebreda, A. R. (2007) *EMBO J.* **26,** 2115–2126

37. Motohashi, H., and Yamamoto, M. (2004) *Trends Mol. Med.* **10,** 549–557

38. Trachootham, D., Alexandre, J., and Huang, P. (2009) *Nat. Rev. Drug Discov.* **8,** 579–591

39. Lee, H. R., Cho, J. M., Shin, D. H., Yong, C. S., Choi, H. G., Wakabayashi, N., and Kwak, M. K. (2008) *Mol. Cell. Biochem.* **318,** 23–31

40. Kang, M. H., Wan, Z., Kang, Y. H., Sposto, R., and Reynolds, C. P. (2008) *J. Natl. Cancer Inst.* **100,** 580–595

41. Cabello, C. M., Bair, W. B., 3rd, and Wondrak, G. T. (2007) *Curr. Opin. Investig. Drugs* **8,** 1022–1037